

Experimental Study on Wing Crack Behaviours in Dynamic-Static Superimposed Stress Field Using Caustics and High-Speed Photography

L.Y. Yang^{1,*}, Q. Sun¹, X.N. Zhao¹ and Y.B. Wang^{1,2}

¹School of Mechanics & Civil Engineering, China University of Mining & Technology (Beijing), Beijing 100083, China

²Department of Mechanical Engineering, University of South Carolina, Columbia, SC 29208, USA

Received 6 April 2014; Accepted 13 July 2014

Abstract

During the drill-and-blast progress in rock tunnel excavation of great deep mine, rock fracture is evaluated by both blasting load and pre-existing earth stress (pre-compression). Many pre-existing flaws in the rock mass, like micro-crack, also seriously affect the rock fracture pattern. Under blasting load with pre-compression, micro-cracks initiate, propagate and grow to be wing cracks. With an autonomous design of static-dynamic loading system, dynamic and static loads were applied on some PMMA plate specimen with pre-existing crack, and the behaviour of the wing crack was tested by caustics corroding with a high-speed photography. Four programs with different static loading modes that generate different pre-compression fields were executed, and the length, velocity of the blasting wing crack and dynamic stress intensity factor (SIF) at the wing crack tip were analyzed and discussed. It is found that the behaviour of blasting-induced wing crack is affected obviously by blasting and pre-compression. And pre-compression, which is vertical to the direction of the wing crack propagation, hinders the crack propagation. Furthermore, the boundary constraint condition plays an important role on the behaviour of blasting induced crack during the experiment.

Keywords: pre-compression stress field, blast-induced wing crack, caustics, stress intensity factor (SIF)

1. Introduction

In deep-level mining, the high initial *in-situ* earth stress plays an important role on all kinds of underground engineering structure. Drilling and blasting operations are widely used in the underground engineering, such as underground spaces and tunnels and shaft excavations. So the rock mass at deep-level mine is in dynamic-static superimposed stress field, which means that the rock fragmentation is produced by the high initial earth stresses and explosive. The first significant experimental study devoted to the influence of static stress field on the wave and gas-generated fragmentation pattern was reported by Kutter and Fairhurst [1] in 1971. They found that the blast-induced cracks grew preferably in the direction of maximum principle stress of dynamic-static superimposed stress field. The problem was theoretically and experimentally explored in two dimensions using PMMA and rock discs. In 1996, Rossmanith and Knasmillner [2] carried out some three-dimensional laboratory-scale experiments in a transparent PMMA. In this study, the fracture propagation in a uniaxial compressive stress field was investigated by a high-speed photography; the fracture pattern displayed an obvious correlation with the direction of its major principal stress. Lu and Chen [3] preformed some excavation sequence and contour blasting experiments in underground powerhouses of hydropower stations to investigate the effects of *in situ* stress on rock fragmentation. Yang [4] used the caustics by high-speed photography to study the blasting-induced crack behavior in initial compression stress field. It is well

recognized that the properties of a rock mass are affected by the properties of rock and its flaws inside, such as joints, faults, microcracks. The initiation and growth of a crack from pre-existing flaws under static loading has been studied both analytically and experimentally [5,6,7]. Lee and Ravichandran [8] studied the wing crack initiation in brittle materials under dynamic loading conditions (impact-induced compression stress) using dynamic photoelasticity. Bhandari and Badal [9] conducted the blasting experiments on a laboratory scale in jointed rock with a single plane of discontinuity. Yang [10,11,12] carried out many laboratory blasting experiments in 5–10 mm-thick PMMA specimens using caustics with a high-speed photography to record the evolution of two-dimensional wing cracks. These wing cracks appeared at the tip of pre-existing microcracks, flaws and joints.

However, relatively less work has been done regarding the wing crack phenomena in dynamic-static superimposed stress fields. The wing crack behaviors in a dynamic-static superimposed stress field, together with the influence of initial static stress (the pre-compressive stress or confining stresses) on a solid materials fracture pattern, is still an open question. In this paper, the wing crack behaviors in a dynamic-static superimposed stress field are experimentally studied using dynamic caustics and high-speed photography.

2. Theoretical analysis

In the linear elastic mechanics, it is assumed that the stress and the displacement of a point in an elastic body applied several loads are complied with the superposition principle. The stress condition of a crack is in a dynamic-static stress

field. The stress intensity factor at a crack tip can be divided into two parts [13], which is given by,

$$K_N^0 = K_N^s + K_N^d \quad (1)$$

Where K_N^s , K_N^d are the static stress intensity factor and dynamic stress intensity factor of the crack tip, respectively; the subscript N represents the crack mode (I, II and III).

A 2D infinite plate model is considered, where a pre-existing crack with the length of $2a$ is under the loads of σ_1 in the lateral direction and σ_2 in the vertical direction. The included angle between the crack and the horizontal axis is θ . A blast hole locates at a distance of d from the crack, which provides the dynamic loading σ_d to initiate the crack.

2.1 Analysis of the effect of the static stress field on the crack tip

As shown in Fig.1, in the static stress field, when the crack starts, the tensile wing crack will firstly form at the pre-existing cracks and then it will propagate to deviate from the original direction and be inclined to the parallel direction of maximum principal stress. In fact, the propagation of a wing crack is a complicated process, which is usually simplified into mode I crack by introducing sliding crack equivalent model, which is proposed by Horii and Nemat-Nasser [6]. In this simplified model, the wing crack can be equivalent to a straight crack, which has a length of $2l$ (l is half the length of the wing crack) and a splitting force of q , as shown in Fig.2. The splitting force q can be given by:

$$q = 2a\tau_n \quad (2)$$

$$\tau_n = \frac{1}{2}(\sigma_1 - \sigma_2)\sin 2\theta - \frac{1}{2}f \times [\sigma_1 + \sigma_2 - (\sigma_1 - \sigma_2)\cos 2\theta] \quad (3)$$

Where τ_n is the crack surface friction; f is the coefficient of friction between the crack faces.

When the angle between propagation direction of the wing crack and the crack surface is φ , the static stress intensity factor of the wing crack tip is:

$$K_1^s = \frac{2a\tau_n \sin \varphi}{\sqrt{\pi(l+l')}} - \frac{1}{2}\sqrt{\pi l} \times [\sigma_1 + \sigma_2 - (\sigma_1 - \sigma_2)\cos 2(\varphi - \theta)] \quad (4)$$

Where l is the half-length of the wing cracks; l' is a constant and $l'=0.27a$.

2.2 Analysis of the effect of the dynamic stress field on the crack tip

The dynamic stress intensity factor is a very complicated physical-mechanical property. Its value is related to the defect size, stress and time. Thereby, there is no unified mathematical theory available to obtain an exactly analytical solution. Broberg [14] proposed an approximate way to analyze this problem. In this theory, the dynamic stress intensity factor is expressed as a function of static stress intensity factor, which is given by:

$$K(t) = k(v)K(0) \quad (5)$$

$$k(v) = (1 - v/c_R)(1 - hv)^{-1/2} \quad (6)$$

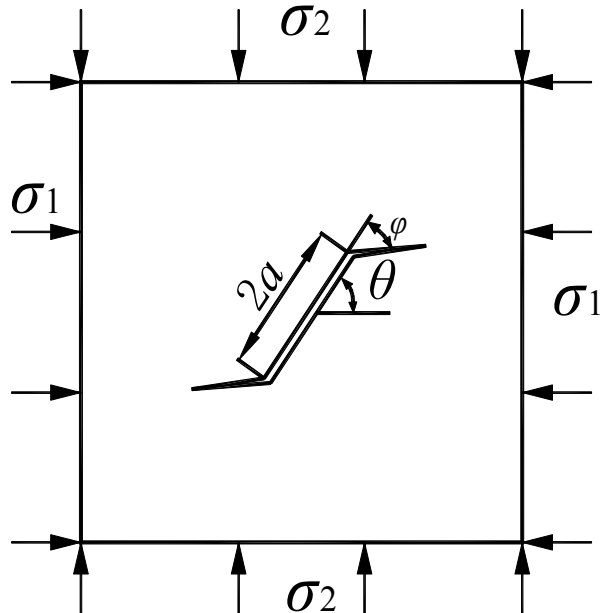


Fig.1. Crack sliding model

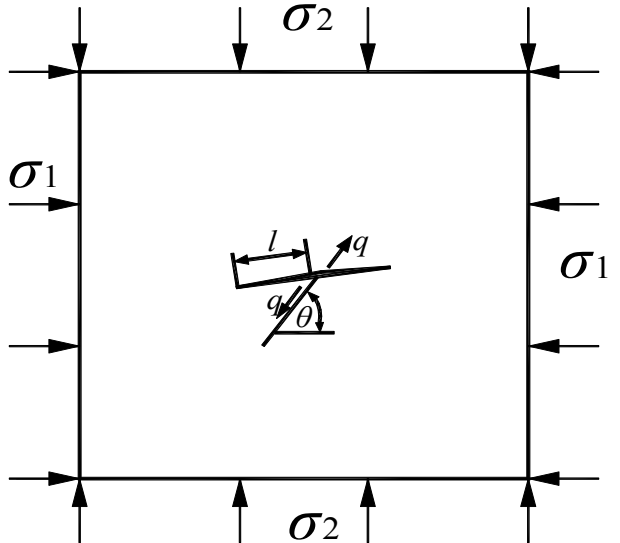


Fig.2. Stress distribution of wing crack propagation

Where $K(t)$ represents the dynamic stress intensity factor while the propagation velocity of the crack is v ; $K(0)$ is the static stress intensity factor; $k(v)$ is a function related to velocity; c_R is the speed of Rayleigh wave; h is the function of the elastic wave.

For the problem of infinite flat plate with a circle hole and penetrating crack, which is $2a$ in length and the inclination of θ , explosive in the hole is detonated to generate plane stress wave, which is considered to be a horizontal dynamic load on the crack. According to the formula (4), the dynamic stress intensity factor under stress wave can be expressed as:

$$K_1^d = \left\{ \frac{2a\tau'_n \sin \varphi}{\sqrt{\pi(l+l')}} - \frac{1}{2}\sqrt{\pi l} \times [\sigma_d - \sigma_d \cos 2(\varphi - \theta)] \right\} k_1(v) \quad (7)$$

Where τ'_n is the dynamic shear stress. It can be expressed as:

$$\tau'_n = \frac{1}{2} \sigma_d \sin 2\theta - \frac{1}{2} f' (\sigma_d - \sigma_d \cos 2\theta) \quad (8)$$

Where f' is the dynamic friction coefficient between the crack faces.

In summary, the compound stress intensity factor in the dynamic-static superimposed stress field can be given by:

$$K_1^0 = \frac{2a \sin \varphi}{\sqrt{\pi(l+l')}} [\tau_n + \tau'_n k_I(v)] - \frac{1}{2} \sqrt{\pi l} \cdot \{ \sigma_1 + \sigma_2 + \sigma_d k_I(v) - [\sigma_1 + \sigma_d k_I(v) - \sigma_2] \cos 2(\varphi - \theta) \} \quad (9)$$

3. Experimental details

3.1 Experimental setup

The experimental optical equipment of multi-spark high speed camera is shown in Fig. 3, which consists of a 4×4 array point light source, a pair of field lens and a 4×4 array camera. The specimen was set between the pair of the lens of the same optic plane. In this equipment, the output aperture of the spark gap should be as small as possible to produce a point light source for obtaining a caustics spot. The light from each spark firstly transmitted through the specimen, and then entered into the camera where the specimen off-focused images were obtained. The synchronizations of the impact load with the sparks are achieved by a time sequence controlled circuit. In this test, the distance between the reference and the specimen planes is 1.5 m. An independent design static-dynamic loading system is employed to simulate the blasting load and the initial compressive stress field. The system is composed of two parts: a static confining pressure setup and a blasting load setup.

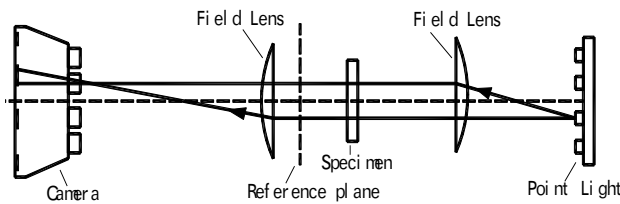


Fig.3. Schematic illustration of a transmitted caustics optical system

3.2 Specimen design and loading scheme

The PMMA plate with a length of 300mm, a width of 300mm and a thickness of 5mm is manufactured. The physical and mechanical parameters are followed: a longitudinal wave velocity of $C_p = 2125$ m/s, a shear wave velocity of $C_s = 1090$ m/s, a dynamic elastic modulus of $E_d = 2.6$ GPa/m², a Poisson's ratio of $\nu_d = 0.32$, an optical constant of $c_t = 0.08$ m²/GN. In order to use the blasting energy efficiently, a notching blasting technology is used by a notched blasthole. The blasthole, with a diameter of 5 mm, a cutting angle of 60° and a cutting depth of 1.5 mm, locates in the center of the specimen. The explosive is a lead azide with a charge of 120 mg. The pre-existing crack is 50 mm in

length, 1.0 mm in width, and 25 mm away from the center of the blasthole, as shown in Fig. 4.

The longitudinal and lateral stresses induced by loads are named as σ_v and σ_h , respectively (as shown in Fig. 4). Four experimental programs were designed with different initial compressive pressure fields in the specimens. This is realized by adding different confining pressure loading programs in every direction. The loading schemes are S-1 ($\sigma_h = \sigma_v = 0$ MPa), S-2 ($\sigma_h = \sigma_v = 0.6$ MPa), S-3 ($\sigma_h = 0.6$ MPa, $\sigma_v = 0$ MPa) and S-4 ($\sigma_h = 0$ MPa, $\sigma_v = 0.6$ MPa), respectively.

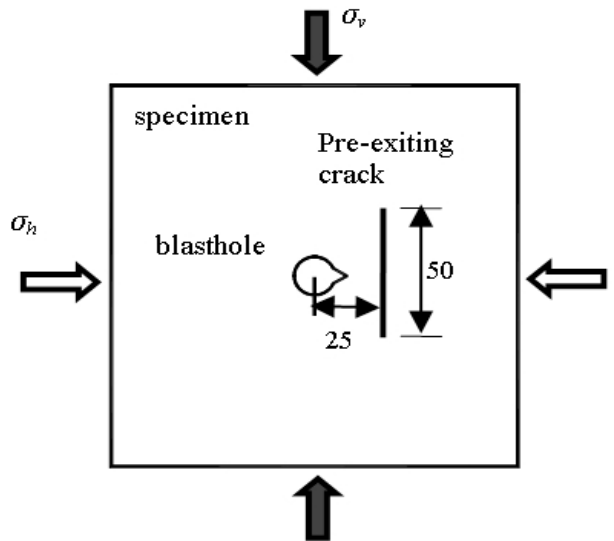


Fig.4. Schematic diagrams of loading and specimen geometry.

4. Evaluation of dynamic fracture parameters

4.1 Determination of the crack growth velocity and acceleration

During crack propagation, the position of crack tip along the initial crack line can be precisely captured by the image. Then, the growth of crack length at different times can be measured. In order to minimize data scattering in the evaluation of fracture parameters, such as crack velocity and acceleration, a data-fitting procedure proposed by Takahashi and Arakawa [15] is used to express the actual crack length $l(t)$, which is a function of ninth order polynomial at time t . It is given by:

$$l(t) = \sum_{i=0}^n l_i t^i \quad (10)$$

Where, the coefficient l_i is determined by the least squares method. Thus, the crack velocity v and acceleration a are determined from the first and second time derivative of the fitted curve $l(t)$, respectively. Those are given by,

$$v = \dot{l}(t) \quad a = \ddot{l}(t) \quad (11)$$

4.2 Determination of dynamic stress intensity factors

The thickness of the plate specimen is uniform before the tests perform is set. The specimen will change non-uniformly in the optical path when the light is transmitted through it. For a specimen made of a transparent material, the change in the optical path is not only due to non-

uniformity in the plate thickness, but also due to the gradient in the refractive index of the material. In experimental solid mechanics, both the gradients in the refractive index and non-uniform thickness variations are related to the gradient of the stress state induced by loads that are applied from the boundary of the initial un-deformed plate. When a collimated light beam is incident on the plate under a certain stress gradient, the refracted rays will form an envelope in the form of a three-dimensional surface. This surface, called the caustic surface, is the locus of points of maximum luminosity in the transmitted light fields. In the experiment, a collimated light beam illuminates the specimen surface, and the transmitted beam is recorded by a camera that focuses on the caustic surface separated from the specimen surface by a small distance, z_0 . In the presence of a crack, the caustic pattern has the characteristic of an approximately dark circular region at the crack tip.

According to the caustics patterns of the propagated crack tip under mode I+II loading, the relation between the characteristic dimensions of the caustic pattern and the mixed-mode stress intensity factor K_I and K_{II} are obtained by the following equation [16]:

$$K_I = \frac{2\sqrt{2\pi}F(v)}{3g^{5/2}z_0cd_{eff}} D_{max}^{5/2} \quad (12)$$

$$K_{II} = \mu K_I$$

Where D_{max} is the maximum transverse diameter of the caustic; z_0 is the distance between the specimen plane and the image plane; d_{eff} is the effective thickness of the specimen; c is the dynamic optical constant, and $F(v)$ is a correction factor that accounts for velocity effects on the distribution of the dynamic stress field for a propagating crack. For practically relevant crack velocity, $F(v)$ is unnecessary, because it is nearly equal to 1.0. μ is a ratio of stress intensity factors.

5. Results and discussion

After experimentation, the images of the specimens are shown in Fig.5. Images of caustic at different time in S-4 experimental scheme are shown in Fig.6.

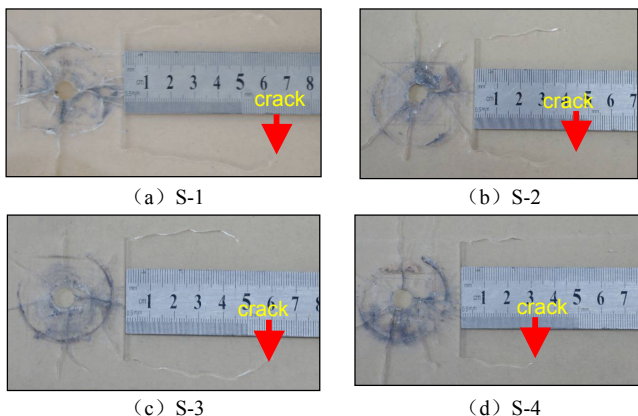


Fig.5. Comparison of blast-induced wing crack propagating path

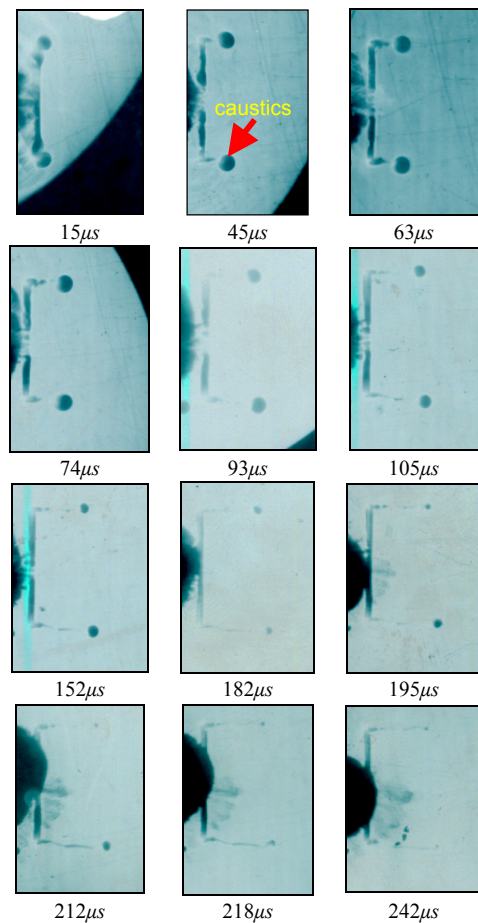


Fig.6. Dynamic caustic spot of S-4

5.1 Comparison of crack path

As can be seen from the Fig.5, two symmetrical blast-induced wing cracks occur at the both ends of the pre-existing crack after blasting in the four loading schemes. The early propagation direction of the crack in different specimen is almost same, but their total cracks length and the later propagation direction of cracks are different from each other. The following discussions focus on analyzing the characteristics of one wing-crack.

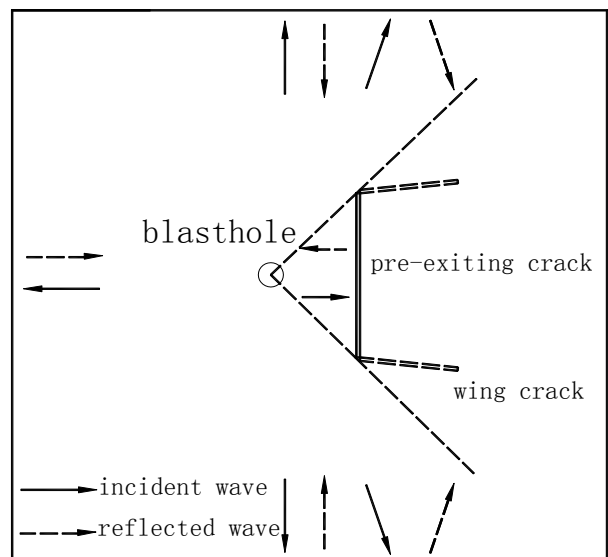


Fig.7. Schematic diagram of stress wave propagation

In the later stage of propagation, a larger difference in the direction appears. The no confining pressure specimen S-1 and the lateral confining pressure specimen S-3 have a very similar crack propagation path, and the propagation direction of wing crack begin to intermediate deflection. This is mainly due to the interaction between stress wave and blasting-induced wing crack, as shown in Fig.7. Because of the pre-existing crack, the stress waves can not go through the crack directly and interact with blasting-induced wing crack, but they can interact with the crack when only emitted by the boundary surface. Moreover, the reflected stress waves formed at the left side of the specimen, rarely encounter with the wing crack, namely, the lateral boundaries reflected stress waves rarely affect the propagation. But, the reflected stress waves generated from the upper and lower interfaces meet, interact with the wing crack, and obviously affect the propagation. The reflected stress waves generated from upper interface mainly interact with the upper wing crack. While the waves generated from lower interface interact with the lower crack. And the asymmetry of the applied load makes the wing crack deviate from the original orientation and approach to the center deflection. Therefore, for the specimen S-1 without confining pressure and the specimen S-3 with lateral confining pressure only, which both have free upper and lower boundaries, the reflected stress waves have same influence on the crack propagation and produce similar propagation path.

The specimen S-2 with confining pressure and the specimen S-4 with only vertical confining pressure have a very similar crack propagation path. During the whole crack propagation, their direction doesn't change obviously like S-1 and S-3, even in the later stages of the propagation. It is because lateral restraints basically have no influence on the crack propagation, while the vertical restraints have obvious influence on the crack propagation. Due to the presence of confining pressure constraints, the incident stress waves not only reflect but also go through, when they encounter the boundary surface. Thus, part of the energy will spread out in the form of transmitted stress waves, and the reflected stress wave energy will be reduced by giving the assumption that the total energy of the incident stress waves is constant.

As can be seen from Fig.5, the propagation length of S-1, S-2, S-3 and S-4 are 68mm, 33mm, 47mm and 30mm, respectively. It should be noted that the crack propagation length of the specimen without confining pressure constraint is the longest, which is 100% larger than that of S-2, 44% larger than that of S-3, 127% larger than that of S-4, respectively. So, the confining pressure constraints could hinder the expansion of wing cracks significantly.

For the horizontal direction of wing cracks, their failure is mainly due to the tensile stress fracture mode I (caustics speckle shape shown in Fig.6), so the stress that is perpendicular to the direction of crack, hinders the expansion of wing cracks. Namely, because of the confining stress, the crack extension per unit length requires a larger driving force and consumes more energy.

In these four constraints confining pressure loading schemes, the direction of specimen S-2 and specimen S-4 are both perpendicular to that of crack propagation. While the specimen S-1 and specimen S-3 both has no load on the propagation direction. Therefore, the total propagation length of the wing crack for S-2 and S-4 are shorter than those of S-1 and S-3 under the same total energy of crack driving force.

5.2 Crack velocity

From the Fig.5 and 6, the characteristics of two wing crack in each specimen are same, so analyzing one of the two wing crack is fine. According to the positions of the crack tip in the pictures at different times, the relationship between crack length and time is drawn, as shown in Fig.8. Then the speed of crack growth curves can be obtained through the fitting method described above, as shown in Fig.9. It proves that the speed trends of crack propagation for four specimens are consistent whether the confining pressure exists or not. From crack initiation, the speed rises straightly, up to the maximum speed at 50μs, then declined gradually. However, in every stages of crack propagation, the speed value and change value for all specimens are different.

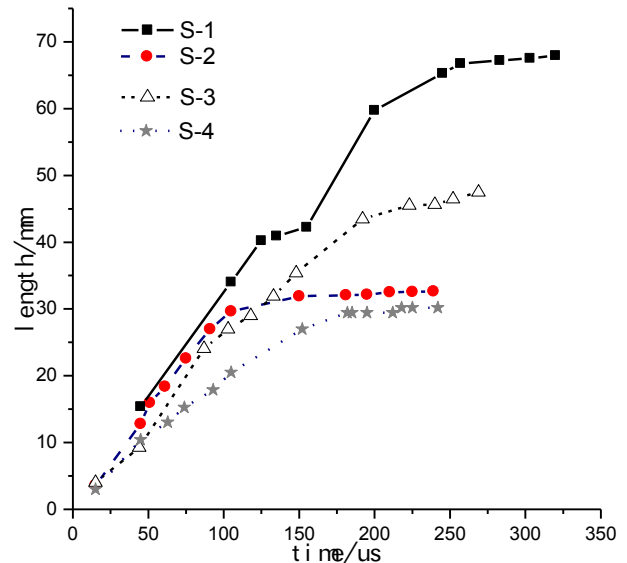


Fig.8. Curve of crack length vs. time

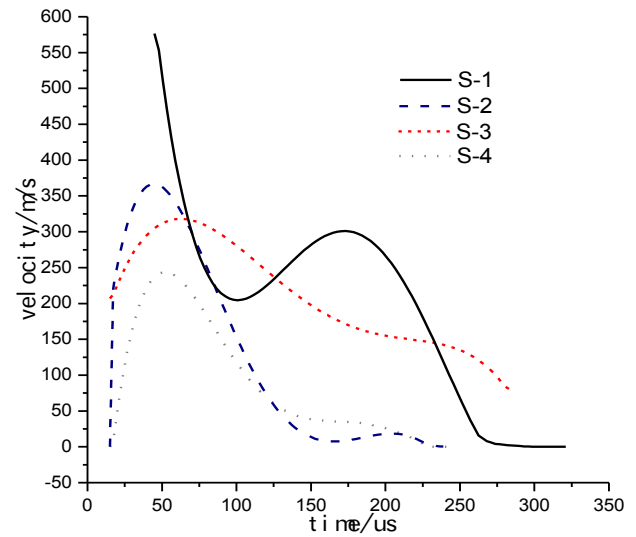


Fig.9. Curve of velocity vs. time

As shown in Fig.9, for the specimen S-1 without confining pressure, the crack velocity change is not recorded before 45μs. The speed reaches the maximum value of 576m/s at 45μs, decreases straightly, down to 205m/s at about 100μs, then starts to rise again, up to 300m/s at 173μs, and declines until the speed reaches to zero at 270μs. For the specimen S-2 with the confining pressure, the speed is up to

418m/s around 45μs, and decreases straightly to zero at 150μs, then the crack stops. For the specimen S-3 with only lateral constraints, the speed reaches a maximum speed of 318m/s at 52μs, and then begins to decline, while the crack stops at 190μs. For the specimen S-4 with vertical confining pressure, the speed curve is similar to that of S-2. It reaches a maximum speed of 245m/s at 50μs, then begins to decline, down to zero at 170μs.

After analyzing the velocity changes of the wing crack for all specimens, it found that, compared with the other specimens, velocity curve of specimen S-1 is obvious different and has more fluctuation, including two peak speeds. The reason is that the other specimens have different confining constraints that dissipate more energy in the expansion process. Meanwhile, compared with the free edge interface, the reflected stress wave at the constraint boundary surface is relatively reduced, which weakens the interaction between the stress wave and the wing crack, so the propagation speed of cracks does not rebound significantly.

5.3 Evolution of dynamic stress intensity factor

According to the caustics pictures, the maximum diameter of the caustics speckle is measured. It could be substituted into a formula, and the dynamic stress intensity factor (SIF) values at different times can be calculated, as shown in Fig.10. It shows that, the trends of the dynamic stress intensity factor under different confining pressures are similar. The SIF value is in a gradual process of growth, and then begins to decline after reaching the peak.

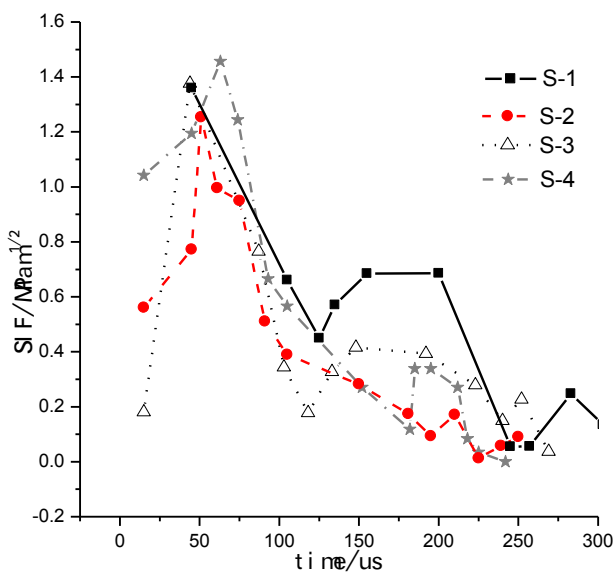


Fig.10. Curve of SIF vs. time

The peak value of stress intensity factor for specimen S-1, $1.36\text{MPa}\cdot\text{m}^{1/2}$, occurs at about 45μs. Then the curve starts to decrease gradually, but rebounds slightly at around 120μs, then decreases again. This is mainly because the reflected stress wave interacts with the propagation crack tip, and part of the reflected stress wave energy passes to the crack, which increases stress concentration in crack tip, and the value of the dynamic stress intensity factor is enhanced. Moreover, the reflected stress wave consists of longitudinal wave and shear wave, which have complex interactions with crack tip. So the stress intensity factor fluctuates.

The stress intensity factor for specimen S-2 is up to $1.25\text{MPa}\cdot\text{m}^{1/2}$ at about 50μs, starts to decline gradually with a small fluctuations at the 200μs. The main reason for the different phenomena between specimen S-1 and specimen S-2 is the existing of the surrounding pressure constraints. The incident stress waves are not only reflected but also go through, when they encounter the boundary surface. Thus, part of the energy will spread out in the form of transmitted stress waves, which decreases the interaction with the moving crack, so crack tip stress concentration does not significantly enhance, and the stress intensity factor values decrease gradually.

The peak value of stress intensity factor for specimen S-3, is $1.38\text{MPa}\cdot\text{m}^{1/2}$ at about 45μs. Then the curve rebounds at the 120μs, which is similar with the specimen S-1. As the direction of lateral confining pressure load is parallel to that of the crack propagation, the effect of the lateral confining pressure on the cracks is ignored. Meanwhile, the stress wave that interacts with the crack is mainly the reflected stress wave from the upper and lower boundary of the interface, which is same as the specimen S-1. The interaction increases the stress concentration factor.

The stress intensity factor for specimen S-4 is up to $1.45\text{MPa}\cdot\text{m}^{1/2}$ at about 63μs, begins to decline gradually after the peak, rebounds at the 180μs, which is similar to that of the specimen S-2 because of the similar vertical confining loads.

According to the comparison and analysis for the four specimen test results, the peak values of dynamic stress intensity factors for all specimens reach at around 50μs, and change a little bit within a small range. From the interaction between the stress wave and pre-existing crack tip to stress wave reflected from the interface meeting the wing crack, the change values of dynamic stress intensity factor in wing crack tip have the same trends, and their differences are not obvious, this is mainly because, the confining pressure applied on the boundary is small.

6. Conclusions

(1) The blasting fracture damage effects of deep rock mass are dominated by the blast loading, *in-situ* stress field, natural micro-cracks.

(2) The behavior of blasting-induced wing crack is obviously related to the *in-situ* stress field. The *in-situ* stress field, which is perpendicular to the crack propagation, hinders the propagation, reduces the crack tip stress concentration, and shortens the wing crack propagation distance. But the *in-situ* stress field with the direction of being parallel to that of crack propagation, has little influence on crack propagation behavior.

(3) Confining pressure device changes the boundary condition of the specimen. Part of energy spread out in the form of transmitted stress wave, which reduces the energy of reflected stress wave and weakens the interaction of stress waves and cracks reflection.

(4) The loading value applied by the static-dynamic loading setup is small. And the condition that the direction of the confining pressure is orthogonal to that of the wing crack during the tests only is considered. So the conclusion is limited. It is still an urgent need to further research the effect of *in-situ* stress field on the blasting-induced wing crack.

Acknowledgements

The authors are grateful for the financial supports from the PhD Programs Foundation of Ministry of Education of

China (PPFMEC) in 2012 (No. 20120023120020) and the National Natural Science Foundation of China (NSFC) in 2012 (No.51134025).

References

1. H.K. Kutter, C. Fairhurst, “On the fracture process in blasting”, *International Journal of Rock Mechanics and Mining Sciences & Geomechanics Abstracts* 8(3), 1971, pp. 181-202.
2. H.P. Rossmannith, R.E. Knasmillner, A. Daehnke and Jr. L. Mishnaevsky, “Wave propagation, damage evolution, and dynamic fracture extension. Part II. Blasting”, *Material Science* 32(4), 1996, pp. 403-410.
3. W. Lu, M. Chen, X. Geng, D. Shu and C. Zhou, “A study of excavation sequence and contour blasting method for underground powerhouses of hydropower stations”, *Tunnelling and Underground Space Technology* 29, 2012, pp. 31-39.
4. L. YANG, R. YANG, P. HU and Y. SONG, “Experimental study on the effect of initial compression-stress field on blast-induced crack behaviors”, *Journal of China Coal Society* 38(3), 2013, pp. 404-410.
5. M.F. Ashby, C.G. Sammis, “The damage mechanics of brittle solids in compression”, *Pure and Applied Geophysics* 133(3), 1990, pp. 489-521.
6. H. Horii, S. Nemat-Nasser, “Brittle failure in compression: splitting, faulting and brittle-ductile transition”, *Philosophical Transactions for the Royal Society of London A: Mathematical and Physical Sciences* 319(1549), 1986, pp. 337-374.
7. F. Lehner, M. Kachanov, “On modelling of ‘winged’ cracks forming under compression”, *International Journal of Fracture* 77(4), 1996, pp. 69-75.
8. S. Lee, G. Ravichandran, “An investigation of cracking in brittle solids under dynamic compression using photoelasticity”, *Optics and Laser Engineering* 40(4), 2003, pp. 341-352.
9. S. Bhandari, R. Badal, “Post-blast studies of jointed rocks”, *Engineering Fracture Mechanics* 35(1), 1990, pp. 439-445.
10. R.S. Yang, L.Y. Yang, Z.W. Yue, T.S. Xiao, J.C. Dong and X.C. Niu, “Dynamic caustics experiment of crack propagation in material containing flaws under blasting load”, *Journal of China Coal Society* 34(2), 2009, pp. 187-192.
11. R. YANG, Z. YUE, T. XIAO, J. DONG and L. YANG, “Dynamic caustics experiment on crack propagation of jointed medium fracture with controlled blasting”, *Chinese Journal of Rock Mechanics and Engineering* 27(2), 2008, pp. 1-5.
12. R. YANG, X. NIU, H. SHANG and L. JING, “Dynamic caustics analysis of crack in sandwich materials under blasting stress wave”, *Journal of China Coal Society* 30(1), 2005, pp. 36-39.
13. S. YIN, “Theory of fracture damage and its application”, Tsinghua University Press, Beijing, 2010.
14. P. Burgers, “Dynamic linear elastic crack propagation in anti-plane shear by finite differences”, *International Journal of Fracture* 16(3), 1980, pp. 261-274.
15. K. Takahashi, K. Arakawa, “Dependence of crack acceleration on the dynamic stress-intensity factor in polymers”, *Experimental Mechanics* 27(2), 1987, pp. 195-199.
16. G.A. Papadopoulos, “Fracture mechanics: the experimental method of caustics and the Det.-Criterion of fracture”, Springer-Verlag, London, 1993.